Preparation of
Hazard, Vulnerability & Risk Analysis Atlas and Report for the State of Himachal Pradesh

Earthquake Hazard Risk Assessment

Composite Final Draft Report

(T6)

Prepared for

Disaster Management Cell, Department of Revenue

Government of Himachal Pradesh, Shimla

Prepared by

TARU

TARU Leading Edge Pvt. Ltd.

New Delhi and Ahmedabad, India

March 2015

VOLUME GUIDE

This series of reports present detailed technical and methodological documentation of the study entitled "Preparation of Hazard, Vulnerability & Risk Analysis Atlas and Report for the State of Himachal Pradesh" for DM Cell, Revenue Department, Himachal Pradesh.

Hazard Risk

This volume contains Technical papers on hazard risk assessment due to natural and man-made hazards within Himachal Pradesh as presented below.

1. Avalanche Hazard Risk
2. Climate Change & Flood Hazard Risk
3. Drought Hazard Risk
4. **Earthquake Hazard Risk**
5. Environmental & Industrial Hazard Risk
6. Forest Fire Hazard Risk
7. GLOF Hazard Risk
8. Landslide Hazard Risk

Vulnerability and Risk

This volume contains Technical papers on the Vulnerability and Risks to key elements at risk within Himachal Pradesh as presented below.

1. Socio-Economic Vulnerability and Risk
2. Building Vulnerability and Risk

Hazard Risk

Earthquake Hazard Risk Assessment

Composite Final Draft Report

(T6)

Contents

List of Figures

No table of figures entries found.

List of Tables

No table of figures entries found.

Abbreviations

FRF	Frequency response function
GCMT	Global Centroid Moment Tensor
GSI	Geological Survey of India
HFT	Himalayan Frontal Thrust
IMD	India Meteorological Department
ISC	International seismological centre
ITS	Indus Tsangpo suture
MASW	Multi-channel analysis of Surface Waves
MBT	Main Boundary thrust
MCT	Main central thrust
MFT	Main Frontal thrust
M_w	Moment Magnitude
NDMA	National Disaster Management Authority
PGA	Peak Ground Acceleration
PSHA	Probabilistic Seismic Hazard Assessment
THF	Trans Himadri Fault
UHRS	Uniform hazard response spectrum
USGS	United States Geological Survey

Executive Summary

Chapter 1: Seismic Hazard of Himachal Pradesh

1.1 Introduction

The state of Himachal Pradesh with Shimla as the capital city lies in the Himalayan region. There has been an increase in population and infrastructure developments in the state of Himachal Pradesh in the last few decades. As per census 2011, the total population of HP is 6.8 million, which is about 12.81 % growth since last census of 2001. The state of HP comprising of twelve districts covers an area of about 55,673 sq. km. with the population density registered at 123 people per sq. km. The Indian standard code of practice for earthquake resistant design of structures, IS 1893 (2002), has identified seven districts of HP in zone of most severe (Zone V) seismic hazard with the design peak ground acceleration as 0.36g. The remaining five districts lie in zone of high seismic hazard (Zone IV) with design PGA as 0.24g. This region has felt large earthquakes in the past. The 1905 Kangra earthquake (M_w 7.8) caused severe damage in Kangra and Dharmashala region of HP. Apart from this event; damages have been reported during the 1975 event (M_w 6.8), 1991 Uttarkashi earthquake (M_w 6.8) and 1999 Chamoli (M_w 6.5) earthquake. In the present times, with sharp increase in population and urbanization, any such event would cause far more destruction. Besides, several fast track planned developments of many towns in this region have been taken up, in the recent times, which need a reliable seismic input for planning and design.

Due to continuous efforts by different researchers, there is considerable improvement in our knowledge about seismo-tectonic characterization and relevant data in India. For instance, Geological Survey of India (GSI) has compiled and integrated all available data on geological, geophysical and seismological attributes for the entire country and has brought out the Seismotectonic Atlas of India and its Environs (GSI 2000). Similarly, paleoseismic investigations and identification of historical events (Oldham 1883; Iyengar *et al.*1999) helps us to build a robust earthquake catalogue. Further, important information on the quality factors of different regions of India are available (NDMA 2011). Integrating all the above scientific information, it is possible to carry out PSHA of HP. Mapping of the PSHA result will be useful to Engineers, planners and to agencies interested in disaster mitigation.

1.2 Scope of Work

The scope of the present study is to develop surface level PSHA maps of PGA and spectral acceleration for 12 important towns in HP over a grid of 200m x 200m. It also includes estimating the sub surface soil profiles at various locations in HP by conducting geophysical test based on the Multi-channel analysis of Surface Waves (MASW) method. Uniform hazard response spectra (UHRS) defined as the acceleration response spectrum which has the same annual probability of exceedance at all periods (frequencies), including the zero period where S_a= ZPA= PGA are developed for 12 important towns in HP following PSHA. In order to obtain a UHRS, one has to develop ground motion prediction equations relating spectral amplitudes to magnitude and distance. In the present study, the attenuation of surface level spectral acceleration as applicable to

Himalayan region and Indo-Gangetic plain has been obtained by generating synthetic data through the stochastic seismological model of Boore (2009).

After deriving the ground motion relations, seismic hazard curves for spectral acceleration are derived by performing probabilistic seismic hazard analysis (PSHA). These correspond to return periods of 10, 25, 100, 500 and 2500 years for sites in HP. Uniform hazard response spectra (UHRS) are computed and are also presented for different site conditions. Surface level hazard maps are estimated for entire HP at grid intervals of 200m x 200m size.

1.3 Tectonic Setting of the Region

Estimation of seismic hazard requires identification of geological and tectonic zones in the 500 km region around the site. The generalized tectonic map of India is shown in Figure 1. Indian subcontinent can be divided into three physiographic divisions namely the Himalayas, Indo-Gangetic plains and peninsular India (Valdiya 2010). Of these three divisions, Himalaya is seismically the most active region and HP lies in this region. Himalaya is 2500 km long and the width varies from 250 to 300 km from Kashmir in the north-west to Arunachal Pradesh in the north-east. Himalayan arc is convex southwards with Hazara syntaxis marking the western extremity and the Siang syntaxis marking the eastern extremity. The Himalayan arc meets Pamir–Hindukush region and the Burmese arc at its western and the eastern ends, respectively. The Himalayan Mountain is believed to have been formed 50–60 million years ago due to the collision of Indian plate with Eurasian plate along the Indus Tsangpo suture (ITS). Due to this collision, there is a continuous build-up of strain which makes Himalaya seismically active. This collision gives rise to the formation of active faults like the Trans Himadri Fault (THF), Main central thrust (MCT), the Main Boundary thrust (MBT) and the Main Frontal thrust (MFT). These faults run along the entire length of Himalaya.

The MCT dips 30^0 to 50^0 northwards and separates the Greater Himalaya from Lesser Himalaya. The MBT dips 300 to 500 northwards and separates the Lesser Himalaya and Outer Himalaya (Kayal 2008). The MFT separates the Outer Himalaya from the Indo-Gangetic plain. Apart from these major faults, there are a number of faults present in this region. The thrust faults in the Himalaya divide the region into four geological zones namely the Siwalik ranges, lesser Himalaya, great Himalaya and Tethys domain. The Siwalik ranges which defines the southern boundary of the Himalayas contain the sediments deposited by ancient Himalayan rivers. The elevation of Siwalik ranges lies in between 0.25 km to 0.8 km (Figure 3). The rock formations in lesser Himalaya zone are typically upper Tertiary molassic sedimentary deposits. The lesser Himalaya which lies in between MBT and MCT consists of mostly palezoic sedimentary rocks. The average elevation in lesser Himalaya is 2.5 km. The Great Himalaya which is the most northerly sub-province comprises of crystalline metamorphic and igneous rocks. The average elevation in this geological zone is about 5 km. The formations are highly folded and thrusted in the areas north of the MBT.

The Indo-Gangetic plain also known as Himalayan foredeep lies in between peninsular shield and the Himalayan region (Figure 1). This East-West tectonic basin is characterized by several hidden faults and ridges in the basement of the Ganga basin (Gansser 1974; Valdiya 1976). The Delhi-Haridwar ridge which is demarcated by a pair of faults is the continuation of the Aravali Mountain into the Himalaya through Haridwar. Similarly Faizabad ridge and Munger-Saharsa ridge denotes the prolongation of the Bundelkhand and Sapura massifs. All the ridges are bounded by faults and are in tectonic

continuation from the Indian shield. These faults have oblique and transverse alignment across the Himalayan tectonic trend. Gansser (1974) pointed out that Gangetic plain is not a sediment- filled fore-deep, and it represents the depressed part of the peninsular shield in which several hidden faults exist.

Figure 1: Seism tectonic Features of Himachal Pradesh

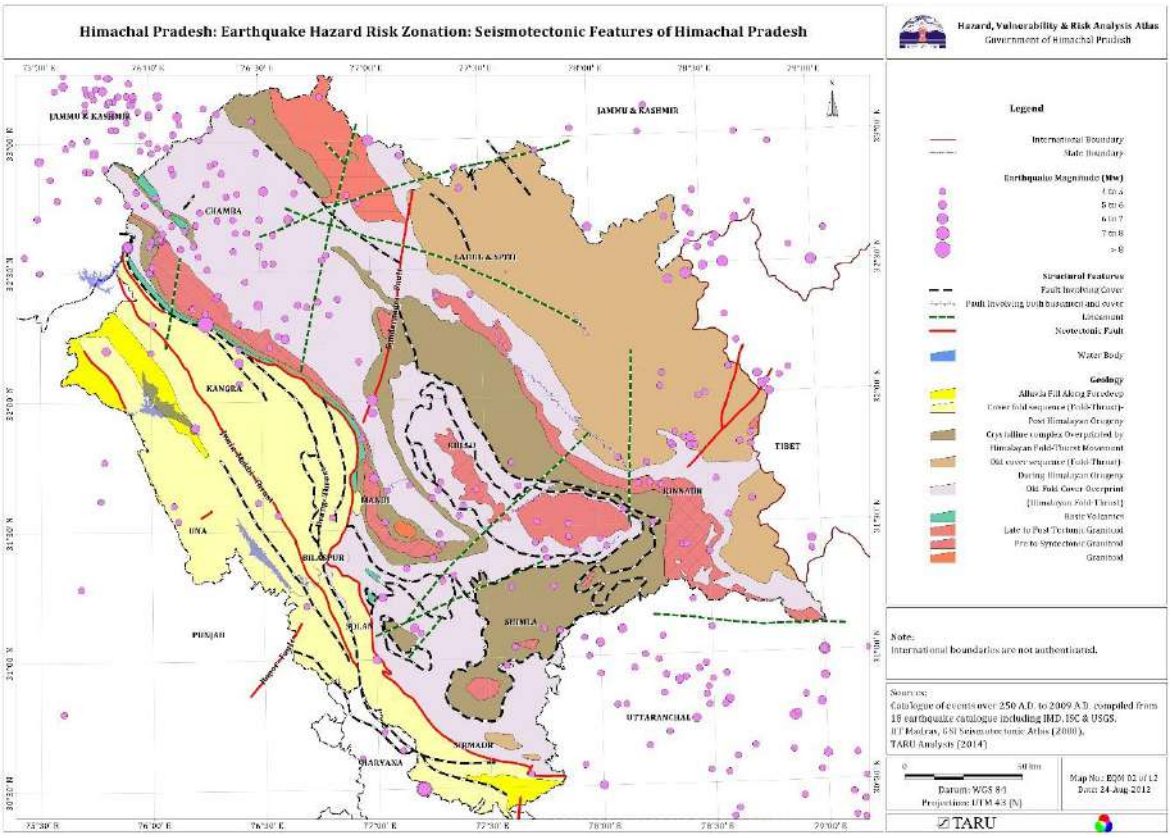

The earthquake activity in the Gangetic plain is broadly associated with strike-slip faulting (Gupta 2006). The Gangetic plain is moderately seismic when compared to the Himalaya (Quittmeyer and Jacob 1979). The faults in the Indo Gangetic plain region exhibit a NE–SW trend and are transverse to the Himalayan chain. The Indo-Gangetic region consists of the vast alluvial plains of the rivers Indus and Ganges. The sagging of land during collision of Indian and Eurasian plate created this geological zone. The Indo-Gangetic region is filled by sediments flowing from both the Himalayas and peninsular shield regions. The thickness of the alluvial deposits is of the order of 1.5-6 km and conceals the solid geology of its basement. The average elevation in this region is about 200 m.

1.4 Earthquake Catalogue

The first step in PSHA is to develop seismicity database of the region. A comprehensive database of location, date and magnitude of past earthquakes is required to understand the seismic status of the region. In the past several investigators attempted to prepare earthquake catalogues for the Indian subcontinent. Notable past efforts in collecting earthquake data for India are by Oldham (1883), Chandra (1977, 1992); Bapat *et al.* (1983), Guha and Basu (1993), Iyengar *et al*. (1999), Rao (2005), and Raghukanth (2011). Oldham was perhaps of the earliest to create an earthquake catalogue for India. A list of significant Indian earthquakes up to 1869 was prepared by Oldham (1883). Quittmeyer and Jacob (1979) prepared a list of Himalayan earthquakes. The catalogue of Bapat *et al*.

(1983) lists about 40 earthquakes in India and its neighbouring region prior to 1800 AD. Chandra (1992) compiled 711 events from the Himalayan region for the period 1505-1986. Iyengar *et al.* (1999) carried out an intensive search of ancient Indian literature for earthquake related information. They identified 38 damaging events in India in the medieval period. Ambraseys and Jackson (2003) identified seven historical events with estimated magnitudes M_w >7 in North India and Tibet. Rao (2005) reviewed several earthquake catalogues prepared for the Indian region and identified fifty important events from 1250 BC to 1963 AD. Pakistan Meteorological Department compiled a list of 58 historical events during AD 25-1905 that occurred in Kashmir and in Pakistan. Ambraseys and Bilham (2009) searched historical Persian documents, British and French Consular reports to identify 52 earthquakes in Afghanistan for the period AD 734-2004. Apart from these historical events, paleo-seismic investigations have been carried out by several investigators to identify the location, time and size of the prehistoric events. These events can be used to supplement historical and instrumental data (McCalpin 2009). Since the recurrence intervals of large and great earthquakes exceed the duration of instrumental and historical records, prehistoric events identified by paleo-seismic investigations would be valuable in building up the earthquake catalogue. Kumar *et al.* (2001) carried out paleo-seismic investigations on the Himalayan Frontal Thrust (HFT) and obtained evidences for a great earthquake (M_w >8) in 260 AD and two major events (M_w >7) in 1294 AD and 1423 A.D near Chandigarh. Investigations by Malik *et al.* (2003) support the identification of the above three HFT events. Lave *et al*. (2005) obtained geological evidences for an earthquake of magnitude (M_w >8.5) on HFT *c* 1100 AD in Far East Nepal. The most accurate and complete information on instrumental earthquakes for India is from permanent global seismic network observations operated by International seismological centre (ISC). This data from 1922 to till date is available in the ISC website (http://www.isc.ac.uk/). The USGS (http://neic.usgs.gov/) website also contains information for location, date, origin time and magnitude. This is considered to be one of the reliable data repositories since 1973. Apart from these global databases, the IMD data base is comprised of historical and instrumentally recorded earthquakes. Only local magnitude ML is assigned to the recorded earthquakes. Recently for the PSHA work of NDMA, Iyengar and Raghukanth have assembled all India catalogue containing all known events of magnitude $M_w \geq 4$ for the region (2^0- 40^0 N; 61^0-100^0 E). A catalogue containing events of magnitude $M_w \geq 4$ for the region are collected from all the above sources. Many times in the past literature only MMI values are reported. For the sake of uniformity and ease in reference, such values have been converted to magnitude numbers using the empirical relation M_w = (2/3 MMI+1). All the instrumental magnitude values have been converted to moment magnitude (M_w) before further analysis. Recently, Scordilis (2006) processed 20,407 global earthquakes from ISC, USGS and Global Centroid Moment Tensor (GCMT, http://www.globalcmt.org) database and derived empirical equations to convert surface wave magnitude, M_s and body wave magnitude, mb to moment magnitude. The derived relations are

M_S - M_W

$$M_w = 0.67M_S + 2.07,\ 3.0 \leq M_S \leq 6.1$$

$$M_w = 0.99M_S + 0.08,\ 6.2 \leq M_S \leq 8.2 \quad (1)$$

mb - M_w

$$M_w = 0.85m_b + 1.03,\ 3.5 \leq m_b \leq 6.2 \quad (2)$$

The body wave magnitude saturates after 6.2. The relation of Idriss (1985) has been used for converting local magnitude (ML) to M_w. The catalogue assembled for HP starts with the 25 AD Taxila earthquake in Pakistan with an approximated M_w of 7.5. All events of magnitude greater than or equal to 4 known up to 31st December 2012 are included in the catalogue. A total of 5958 events have been compiled to estimate seismic hazard for HP. Epicenters of these earthquakes are plotted in Figure 2.

Figure 2: Himachal Pradesh & its Environs - Main Earthquake Events

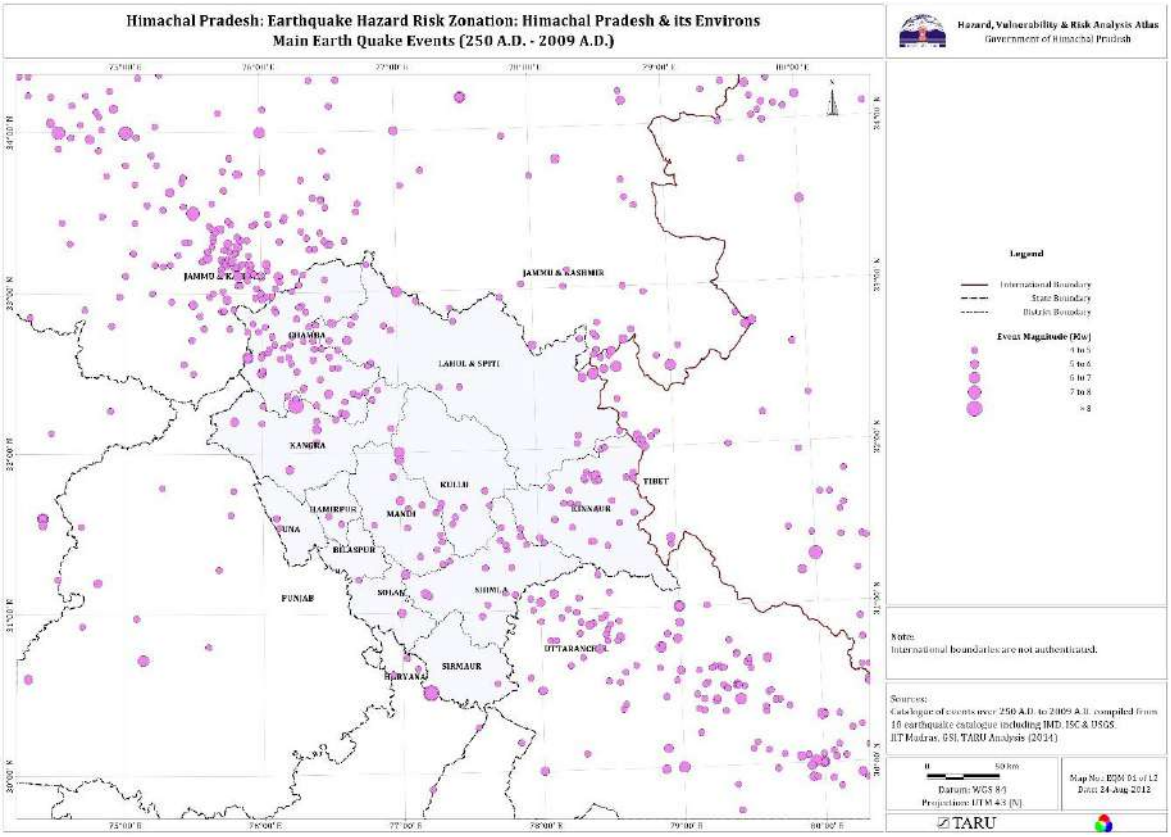

This figure immediately provides a synoptic view of the spatial pattern of the seismicity in the controlling region. As per the available data, Himalayan and Indo-Gangetic seismic belt influences maximally the seismic hazard at HP.

1.5 Seismotectonic Map

Seismotectonic maps for HP have been prepared using the Seismo-tectonic Atlas of India (GSI 2000). These drawings have been also digitized using MATLAB. These drawings are prepared such that all the important seismo-tectonic features within the radius of 500 km around the HP state are captured. The causative fault map for HP is shown in Figure 5. For PSHA, it is necessary to delineate the spatial structure of the seismic zones and the faults within these zones that can be associated with past epicenters. The fault map and seismicity map shows that there are some regions that are more active than others. This activity is correlated with the number of occurrence of past earthquakes and also with the presence of faults and lineaments. There is a possibility that not all past epicenters can be uniquely identified with particular faults. This gives rise to the postulation of diffuse aerial sources in some places to be the cause of seismic activity. However, for the purpose of the present work, it has been accepted that only line sources will be considered and all known activity will be attributed to mapped faults only. The distribution of faults varies spatially

as seen from Figure 5. Some specific patterns can be recognized about the faults and epicenters being dense in some regions. This pattern and the known tectonic disposition can be used to demarcate seismic source zones for further work. Recently NDMA (2011) document on PSHA map of India divides India into 32 homogeneous seismic source zones based on historical seismicity, tectonic features and geology. These zones along with the faults within each zone are shown in Figure 6. It can be observed that the seismic hazard of HP is controlled by events occurring on faults located in western Himalaya, central Himalaya and Indo-Gangetic plain.

1.6 Regional Recurrence

After developing the earthquake catalog, the next step in seismic hazard analysis is to quantify the seismic activity in the source zones by developing earthquake recurrence relations. The seismic activity of a source zone is characterized by the Gutenberg-Richter (G-R) recurrence relation as:

$$\log_{10} N(m) = a - bm \tag{3}$$

Here, *N(m)* is the number of earthquakes greater than or equal to magnitude m. The *(a, b)* values characterize the seismicity of the region. The seismic hazard at any site is controlled by the parameters *(a, b).* Knopoff and Kagan (1977) demonstrated that an upper bound magnitude (Mmax) has to be introduced if the G-R relation is to be applied further in a realistic fashion.

1.6.1 Declustering and Completeness Study

Estimation of the recurrence parameters *(a, b)* assumes the sample data series to be temporally statistically independent. Aftershocks and foreshocks are dependent on the main shock and hence such events get clustered in a general catalogue. The widely used declustering approach is of Gardner and Knopoff (1974) as modified by Uhrhammer (1986). This method is used in the present study to remove time-dependent events from the earthquake catalogue. A total of 2970 foreshocks and aftershocks have been removed from the catalogue.

The total number of events in each seismic zone is reported in Table 1. The earthquake catalogue for Himachal Pradesh developed in the present study is a combination of instrumental, historic and pre-historic data. As such completeness of magnitudes in time has to be established before proceeding further. Here the widely used procedure proposed by Stepp (1972) is applied to determine the interval in a magnitude class over which the class is complete. The earthquake data is grouped into seven magnitude classes namely, $4M_w<5$, $5M_w<6$, $6M_w<7$, $7M_w<8$ and $8\ M_w<9$. With a time interval of 10 years, the average number of events per year in each magnitude range is determined. If x_1, x_2, ...x_n are the number of events per year in a magnitude range, then the mean rate for this sample is

$$\chi = \frac{1}{n}\sum_{i=1}^{n} x_i \tag{1}$$

where, *n* is the number of unit time intervals.

The variance is given by

$$\sigma_x^2 = \frac{x}{T} \quad (2)$$

Where *T* is the duration of the sample. If χ were to be constant, σχ would vary as 1/√T. Following Stepp (1972), the standard deviation of the mean rate as a function of sample length are plotted along with nearly tangent lines with slope 1/√T. The deviation of standard deviation of the estimate of the mean from the tangent line indicates the length up-to which a particular magnitude range may be taken to be complete. The standard deviation shows stability in shorter windows for smaller earthquakes and in longer time windows for large magnitude earthquakes. The standard deviation of the mean of the annual number of events as a function of sample length for the All India data is shown in Figure 7. The analysis shows that data is complete for the sets 4< M<5, 5<M<6, 6<M<7, 7<M<8 and M>8 for the past 50 (1962-2012), 60 (1952-2012), 130 (1882-2012), and 250 (1762-2012) and 600 (1412-2012) years respectively.

1.6.2 Zonal recurrence relation

The simplest way to obtain (a, b) in equation (3) is through least square regression. But, due to the incompleteness of the database, this approach is known to lead to erroneous results. To circumvent this difficulty, Kijko and Sellvoll (1989) proposed a method where the data is organized into two parts called the extreme and the complete part. The extreme part refers to the time period where information on large historical events only is available. The complete part represents the time period in which information on both large as well as small magnitude earthquakes are available. Their method assumes a doubly truncated Gutenberg-Richter relationship and a Poisson model for earthquake occurrences. The uncertainty in the estimation of magnitudes is also incorporated in deriving the parameters. Based on the completeness test, the data set has been divided into complete part (1962-2012) and extreme part (before 1962). The starting point of the extreme part of the catalog for each region is different and taken as the year of first occurrence of an earthquake in that particular region. The parameters of the Gutenberg and Richter equation are found by the maximum likelihood method of Kijko and Sellevoll (1989) assuming a threshold magnitude (m_0) of 4. The uncertainty in the reported magnitudes is taken as 0.5 in the extreme part. For the complete part the magnitude uncertainty is assumed to be 0.3 (NDMA 2011). The three seismic parameters [N(4), b and M_{max}] for all the seven zones are reported in Table 1. The standard deviation of the *b-value* is also reported in this table. The recurrence relation for all the seven seismogenic zones is shown in Figure 8.

1.7 Multi-Channel Analysis of Surface Wave (MASW) tests

After determining the earthquake recurrence relation, the next step is to estimate the local site condition at all the 12 major cities in HP. It is recognized that the shear wave velocity of the top 30 m of the strata is a good indicator of the elastic soil response (IBC 2003). The soil classification based on average shear wave velocity in top 30 meters as per IBC (2003) is reported in Table 2. Hence, in this work, the variation in the shear wave velocity (Vs) profiles in all the district headquarters and few other major cities of Himachal Pradesh is estimated using MASW test. This section briefly outlines the methodology adopted for estimating the shear wave velocity profiles at the test sites. The configuration of the devices and the techniques used for this seismic survey is briefly presented in this section.

1.7.1 Experimental Setup

Figure 9 shows the instruments used for this MASW survey which consists of the following components:

1. Geode Ultra-light exploration seismograph, 24-channel, from Geometrics. Properties: 24 bit, ultra-high resolution 20 kHz bandwidth (8 to 0.02 *ms* sampling), low distortion (0.0005%), low noise (0.2 μV), stacking accuracy (1/32 of sample interval)
2. Geophones, 5-24 nos. of 4.5 Hz frequency
3. Active source: Sledge hammer (8 kg), Strike plate
4. Battery: 12 V

Table 3 lists the general 1D MASW acquisition parameters adopted during this survey. Figure 11 shows the locations of the shots (source) adopted at each of the test sites. It should be noted that three sets of data were stacked to improve the S/N ratio of the data. Also, the geophones located far from the source were set to highest gain to improve the strength of the signal.

1.7.2 Site Selection

The following criterions were followed in the process of selecting suitable test sites.

1. Importance
   a) The site has to be located within the city limit preferably
   b) Near high important structures such as Hospitals, Administrative buildings, bridges, heliports, schools, etc. as they are highly important during emergency scenario and are meant to withstand MCE seismic events.
2. Size

   The site has to be an open ground of minimum 20m x 20m.
3. Noise Free

   Traffic noise – Test sites should be preferably located away from road/rail/air/pedestrian traffic, road works, heavy machinery, etc.

Based on the above criteria, the MASW tests were conducted in 73 sites located in 12 district headquarters and 9 other smaller cities in Himachal Pradesh. Table 4 lists the cities where the test took place and geographic location of all the test sites are given in Table 5.

1.7.3 Seismic Refraction Survey

Seismic refraction survey is a geophysical technique widely used to characterize the underlying soil strata. In this study, a controlled active source generates the seismic waves and recorded by an array of equally spaced geophones. These geophones record the travel time of the seismic waves and show the refractions waves caused due to the differences in the characteristic property of different underlying soil layers. The active source is a sledge hammer of weight 8 kg. Figure 10 shows a schematic view of the seismic refraction survey carried out at the test sites. The source is always placed at a known offset from the array of receivers. The shot locations are shown in Figure 11. There

are five different locations at which the source is placed while carrying out the MASW tests at each of the test location with an offset distance same as that of the geophone spacing. These positions are along the line with an offset from the first and the last geophone and perpendicular to the line at an offset from the first, middle and last geophone.

The receivers or the geophones are placed in equally spaced linear array and can detect the vertical component of the ground motion caused due to the source. The data from all the geophones are collected by a geode and are sent as digital records to a connected computer. A sample waveform of the acquired data with the shot location at-2 m away from the first geophone is shown in Figure 12. Each of these waveforms indicates a connected channel/Geophone and their distance from the first geophone is marked as the ordinate label. Since this waveform corresponds to the shot position 1, it can be seen that the first geophone has received the first arrival initially and the time taken by the waves to reach the other geophones can be observed from the arrival of the first breaks in the subsequent geophone readings. The collected data are then stacked to improve the S/N ratio (signal-to-noise ratio). The signals are then filtered to remove any ambient noise. In order to perform the refraction analysis, it is important to identify the first break point as **shown in Figure 13.**

These breakpoints indicate the arrival of the waves at the geophone locations and a change in slope of this line indicates the presence of an underlying layer. The data is then transformed into frequency–phase velocity domain also known as the dispersion curve. As shown in **Figure 14**, the dispersion curve reveals the dominant phase velocities versus frequency and is an indicator of the variation of the body wave velocities with the depth. **Figure 15,** shows the dispersion curves before and after eliminating low quality data. Further, on applying inversion techniques, the variation of the shear wave velocity across the soil layers are obtained by comparing with theoretical dispersion curve iteratively. **Figure 16** shows the initial approximate shear wave velocity model and the one obtained through inversion.

1.7.4 Shear wave velocity profiles

In this section, the test results of one dimensional MASW tests performed at 73 test locations covering 12 district headquarters in the state of Himachal Pradesh are presented. Furthermore, the detailed one-dimensional profiles of shear wave velocity variation across the depth and the two-dimensional profiles of the shear wave velocity variation along the length of the test location obtained through interpolation of the 1d profiles are shown in Figures 17.1 – 38.3. Figures 39 to 52 show the topography map of the cities in which the test sites were situated with the Vs30 values of the test sites marked. From the obtained shear wave velocity profile, the Vs30 value, which is the depth averaged shear wave velocity in the top 30 m, is calculated as (IBC 2003)

$$V_{S30} = \frac{30}{\sum_{t=1}^{N}\left(\frac{di}{V_{si}}\right)} \qquad (6)$$

where, N denotes the number of soil layers within the top 30 m, di is the thickness of the i^{th} layer in m and Vsi is the shear wave velocity in the i^{th} layer in *m/s*. The site classification scheme of IBC (2003) is reported in Table 2. The summary of the results of the MASW testing performed at the 73 test sites are summarized in Table 5 along with the site classification for each of the test sites. Based on the results obtained from the MASW

study, the following subsection discusses the observations made for each of the test cities briefly. It can be observed from Table 5 that most of the test sites can be classified as C-Type (50 sites) and D-Type (21 sites) sites.

Bilaspur

As listed in Table 5, the tests were performed at 5 sites. The altitudes of these test sites range from 511 *m* to 687 *m* and the variation in the topographic slope can be seen in Figure 39. This attributes to the variability in the V_{s30} values that range from 391 to 659 *m/s*. But, referring to Table 4, we can assign class C criteria to these sites based on the IBC (2003). Moreover, Figure 17.4 shows the images of soil cross section visible near the test sites 1 & 2 and appears to be made of very dense soil and soft rock and thus confirming to our test results. The shear wave velocity profiles of all the 5 test positions done at the 5 test sites are plotted in Figure 17.1 and Figure 17.2 shows the same at individual sites. The results of these five 1d MASW test are then interpolated to obtain the 2d profiles shows in Figure 17.3.

Chamba

The MASW tests were performed at 5 sites spread across Chamba with one site located on the western side of the river Ravi. The altitudes of these test sites range from 877 m to 976 m and can be seen in Figure 40. The measured V_{s30} values range from 291 to 600 m/s and hence 2 of the sites fall under class D while 3 come under class C of IBC 2003 classification. Figure 18.1.b shows the presence of soft rock near test site 4 justifying its C-type classification. The shear wave velocity profiles of all the 5 test positions done at the 5 test sites are plotted in Figure 18.1.a and Figure 18.2 shows the same at individual sites. The results of these five 1d MASW test are then interpolated to obtain the 2d profiles shows in Figure 18.3.

Dhankar Gompa

The MASW tests were performed at 1 site located within the Dhankar Gompa/Monastery at an altitude 3846 m. The measured V_{s30} value for this site is 413 *m/s* and classified as class C according to the IBC 2003 classification. Figure 19.1.a shows the presence of monastery on a soft rock or dense soil formation & Figure 19.1.b shows the test site. The shear wave velocity profiles of the 5 test positions done at the test site are plotted in Figure 19.2.a. The results of these five 1d MASW test are then interpolated to obtain the 2d profiles shows in Figure 19.2.b.

Dhramshala

All the 5 test sites in Dhramshala are found to be Type-C sites as the Vs30 values range from 432 to 597 *m/s.* The altitudes of these test sites range from 1167 m to 1333m and can be seen in Figure 41. Figure 20.1.b & c shows the soil cross section near test sites 4 & 5 revealing the presence of stiff soil and soft rock. Also, it can be seen from Figure 41 that the highest value is obtained at a site with a higher topographic slope. This is expected as hard rock will be more revealed in the region with large variation in topographic slope. The shear wave velocity profiles of all the 5 test positions done at the 5 test sites are plotted in Figure 20.1.a and Figure 20.2 shows the same at individual sites. The results of these five 1d MASW test are then interpolated to obtain the 2d profiles shows in Figure 20.3.

Hamirpur

The MASW tests were performed at 4 sites spread across Hamirpur and 1 site at near Sujanpur fort. The altitudes of these test sites range from 564 m to 882 m and can be

seen in Figure 42. The measured V_{s30} values range from 227 to 637 *m/s* and hence 1 of the sites fall under class D while the rest 4 come under class C. The lowest value was obtained at a park in a residential area under fully saturated condition after raining, which from the available literature (West & Menke, 2000) means a reduced shear wave velocity. Figure 21.1.a shows one of the test sites in Hamirpur. The shear wave velocity profiles of all the test positions done at the 5 test sites are plotted in Figure 21.1.b and Figure 21.2 shows the same at individual sites. The results of these five 1d MASW test are then interpolated to obtain the 2d profiles shows in Figure 21.3.

Kalpa

The MASW tests were performed at 1 site in Kalpa near Reckong Peo at an altitude of 2770 m. The measured V_{s30} value was found to be 394 *m/s* (class C site). This value is similar to the ones obtained at the nearby Reckong Peo. Figure 22.1.a shows the test site. Figure 22.2.a shows the shear wave velocity profiles of all the 5 test positions done at the test site. The results of these five 1d MASW test are then interpolated to obtain the 2d profiles shows in Figure 22.2.b.

Kangra

The occurrence of the 1905 Kangra earthquake was a good enough reason to perform the MASW test at a site very near the historical monument, the Kangra fort. The site can be classified as Type B as the V_{s30} value measured was 853 *m/s*. Figure 23.1.a shows the test site and the shear wave velocity profiles of all the 5 test positions done at the test site are plotted in Figure 23.2.a while Figure 23.2.b shows the interpolated 2d profile.

Kaza

The MASW test was performed at 1 site in Kaza which is an important town in the region and the sub-divisional headquarters of Spiti. The V_{s30} value has been found to be 699 at the test site and the site classifies as type-C. Figure 24.a shows the shear wave velocity profiles of all the 5 test positions done at the test site while Figure 24.b shows the interpolated 2d profile.

Key Gompa

This monastery lies very close to Kaza at an altitude of 3927 m and the test conducted here shows a Vs30 value of 691 *m/s* which is of type C class. Figure 25.1 shows the Key Monastery with the soil formation nearby. Figure 25.2.a shows the shear wave velocity profiles of the 5 test positions done at the test site and Figure 25.2.b shows the interpolated 2d profile.

Keylong

The MASW tests were performed at 2 sites in Keylong. The measured Vs30 values range from 300 to 493 *m/s* which means type C & type D respectively. Figure 43 shows the topography map of Keylong with the V_{s30} values at the test sites marked. Figure 26.1.b shows the presence of loose rock and stiff soil near test site 1 justifying its C-type classification. Figure 26.1.a shows the shear wave velocity profiles of the test positions done at both the test sites and the same are plotted separately for each of the test site in Figure 26.2. Figure 26.3 shows the interpolated 2d profiles.

Kullu

The MASW tests were performed at 5 sites in Kullu with 1 site on the eastern side of the river Beas. The altitudes of these test sites range from 1195 m to 1313 m as shown in Figure 44. The measured V_{s30} values range from 392 to 591 m/s and hence all of the sites

fall under class C of IBC 2003 classification. Figure 27.1.c, d & e shows the presence of soft rock or stiff soil near test sites 3, 5, 4 justifying its C-type classification. Figure 27.1.a shows one of the test sites and the shear wave velocity profiles of all the test positions done at the 5 test sites are plotted in Figure 27.1.b. and Figure 27.2 shows the same at individual sites. The results of these five 1d MASW test are then interpolated to obtain the 2d profiles shows in Figure 27.3.

Manali

The MASW tests were performed at 4 test sites spread across Manali with one on the eastern side of the river Beas. The altitudes of these test sites range from 1851 m to 2003 m and can be seen in Figure 45 which, as previously mentioned, shows lower Vs30 value as the change in topographic slope is lesser. The measured V_{s30} values range from 416 to 569 *m/s* and hence all of the sites fall under class C similar to the previous case of Kullu located nearby. The shear wave velocity profiles of all the test positions done at the 4 test sites are plotted in Figure 28.1 and Figure 28.2 shows the same at individual sites. The results of these five 1d MASW test are then interpolated to obtain the 2d profiles shows in Figure 28.3.

Mandi

The MASW tests were performed at 4 sites spread across Mandi. The altitudes of these test sites range from 877 m to 976 m and can be seen in Figure 46. The measured V_{s30} values range from 240 to 539 *m/s* and hence 2 of the sites fall under type C & the other 2 fall under type D of IBC 2003 classification. It shall be noted that the lowest value was measured at a site close to the banks of river Beas as can be seen from Figure 29.1.a and was mainly stiff soil with pebbles; hence this justifies a type D classification. Figure 29.1.c shows the site 4 with very stiff soil profile and soft rock but the test was carried out post-rain and hence the test value of 352 *m/s* classifies this site as type D. The shear wave velocity profiles of all the test positions done at the 4 test sites are plotted in Figure 29.1.e and Figure 29.2 shows the same at individual sites. The results of these five 1d MASW test are then interpolated to obtain the 2d profiles shows in Figure 29.3.

Nahan

The MASW tests were performed at 3 sites spread across Nahan. The altitudes of these test sites range from 787 m to 874 m and can be seen in Figure 47. The measured V_{s30} values range from 407 to 486 *m/s* and hence all of the sites fall under type C classification. Figure 30.1.b shows the presence of soft rock near test site 4 justifying its C-type classification. Figure 30.1.b shows the typical soil profile comprised of very dense soil with soft rock that exists typically in Nahan. Figure 30.1.c & d shows the sites 2 & 3 and in the latter figure, some portion of the soil profile is revealed and the presence of dense soil can be seen once again. The shear wave velocity profiles of all the test positions done at the 3 test sites are plotted in Figure 30.1.a and Figure 30.2 shows the same at individual sites. The results of these five 1d MASW test are then interpolated to obtain the 2d profiles shows in Figure 30.3.

Nako

The MASW tests was performed at 1 site in Nako at an altitude of 3594 m and the measured V_{s30} value was found to be 394 m/s which is a type C site. Figure 31.1.a shows the test site which is a pavement founded on soft rock. The shear wave velocity profiles of the shot positions done at the test site are plotted in Figure 31.2.a and Figure 31.2.b shows the interpolated 2d profiles.

Rampur

The MASW test was performed at 1 site located at an altitude of 1027 m and the measured V_{s30} value was found to be 313 m/s and hence the site can be classified as type D. The shear wave velocity profiles at all the shot positions are plotted in Figure 32.1.a and Figure 32.1.b shows the interpolated 2d profiles.

Reckong Peo

The MASW tests were performed at 2 sites in Reckong Peo apart from 1 test conducted at the nearby Kalpa as mentioned earlier. The test sites were at an altitude of 2230 m and can be seen in Figure 48. The measured V_{s30} values were 454 and 348 m/s at sites 1 & 2 and hence they can be classified as class C and class D respectively. Figure 33.1.a & b show the test site 2 and the presence of stiff soil near test site 2 respectively with the latter justifying its D-type classification. The shear wave velocity profiles of all the shot position at both the test sites are plotted in Figure 33.1.c and Figure 33.2 shows the same at individual sites. The results of these five 1d MASW test are then interpolated to obtain the 2d profiles shows in Figure 33.3.

Shimla

The MASW tests were performed at 13 sites spread across Shimla. The altitudes of these test sites range from 1760 m to 2074m and can be seen in Figure 49. The measured Vs30 values range from 254 to 779 *m/s* and hence the site-4 with the V_{s30} value of 779 *m/s* (> 760 *m/s*) is a type B site, sites 1,5,8,9,13 &14 fall under class C while the rest of the 6 sites are type D sites. It can be seen from Figure 49 that most of the sites with high Vs30 values are situated in areas with higher topographic slope variation. Figure 34.1 shows the shear wave velocity profiles of all the shot position at all the 13 test sites and Figure 34.2 shows the same at individual sites. The results of these five 1d MASW test at each site are then interpolated to obtain the 2d profiles shows in Figure 34.3. Figures 34.4 (a-o) shows the test sites 1, 2, 3, 6, 7, 8, 9, 10 and 14. The Figures 2.26.4.d, .e, f., and .l show the soil profiles visible at or near the test site 3, 4, 5 and 11 show that the soil is mostly either very stiff or soft rock type.

Solan

The MASW tests were performed at 5 sites spread across Solan and the altitudes of these test sites range from 1439 m to 1789 m and can be seen in Figure 50. The measured V_{s30} values range from 417 to 520 *m/s* and hence all of the sites can be classified as type C. Figure 35.1 a, b show the soil profiles near the test site 1 and 4. The shear wave velocity profiles of all the shot position at all the test sites are plotted in Figure 35.1.c and Figure 35.2 shows the same at individual sites. The results of these five 1d MASW test at each site are then interpolated to obtain the 2d profiles shows in Figure 35.3.

Sundernagar

The MASW tests were performed at 2 sites in Sundernagar at an altitude of 900 m and can be seen in Figure 51. The measured V_{s30} values were 379 m/s (type C) and 317 *m/s* (type D) at sites 1 and 2 respectively. Figure 36.1.a and b shows the test sites. The shear wave velocity profiles of all the shot position at both the test sites are plotted in Figure 36.1.c and Figure 36.2 shows the same at individual sites. The results of these five 1d MASW test are then interpolated to obtain the 2d profiles shows in Figure 36.3.

Tabo

The MASW test was performed at 1 site at an altitude of 3302 m and the measured value of Vs30 was 542 *m/s* which classifies this site as type C. Figure 37.1.a shows the test site. It can be seen that the V_{s30} value lies within the same range as the other test sites located in the Spiti valley such as Kee Gompa, Kaza and Nako. The shear wave velocity profiles of all the shot position at the test site are plotted in Figure 37.2.a and interpolated 2d profile is shown in Figure 37.2.b.

Una

The MASW tests were performed at 5 sites spread across Una at altitudes of 364 m to 400 m as seen in Figure 52. The measured V_{s30} values range from 183 to 270 *m/s* and hence all of the sites fall under class D of IBC 2003 classification. The shear wave velocity profiles of all the shot position at all the test sites are plotted in Figure 38.1.g and Figure 38.2 shows the same at individual sites. The results of these five 1d MASW test at each site are then interpolated to obtain the 2d profiles shows in Figure 38.3. Figure 38.1.a, e. and f. show the test sites 1, 4 and 3 respectively. Figures 38.1.b, c, d and e show the presence of stiff soil profile in all the test sites which explains the assigned classification of class D.

1.8 Ground Motion Relations

After determining the earthquake recurrence relation and local site condition, ground motion relation valid for the region under consideration has to be derived. Attenuation equation is a key component in PSHA. This equation describes the average or other moments of the random hazard parameter in terms of magnitude and distance. The instrumental database for Himalayan and Indo-Gangetic region is sparse and cannot be used to derive attenuation relationships. Hence, attenuation equations in such regions have to be based on simulated ground motions, instead of a few past recordings. Stochastic seismological model originally proposed by Boore (1983) is a viable alternative and is used worldwide for deriving attenuation relationships in regions lacking strong motion data.

1.8.1 Stochastic Seismological Model

In this method, the rectangular fault plane is divided into N number of sub-faults and each sub-fault is represented as a point source. The Fourier amplitude spectrum of ground motion *[A(r,f)]* due to the j^{th} sub-fault at a site is derived from the point source seismological model, expressed as;

$$A_j(r,f) = CH_jS_j(f)F(f)D(r,f)P(f) \quad (7)$$

where, C is a scaling factor, $S_j(f)$ is the source spectral function, $D(r,f)$, is the diminution function characterizing the quality of the region, $P(f)$ is a filter function, $F(f)$ is the site dependent function that modifies the bed rock motion in the vertical direction and H_j is a scaling factor used for conserving the energy of high-frequency spectral level of sub-faults. In the present study, following Brune (1970), the principal source model $S_j(f)$ is taken as;

$$S_j(f) = (2\pi f)^2 \frac{M_{0j}}{\left[1+(f/f_{0j})^2\right]} \quad (8)$$

where, f_{0j} is the corner frequency and M_{0j} is the seismic moment of the jth sub-fault. The three important seismic source parameters, M_{0j} and f_{0j} and the stress drop ($\Delta\sigma$), are related through;

$$f_{0j} = 4.9 \times 10^{6} \left(N_{Rj}\right)^{-1/3} N^{1/3} V_s \left(\frac{\Delta\sigma}{M_{0j}}\right)^{1/3} \quad (9)$$

where, stands for the shear wave velocity in the source region, corresponding to bedrock conditions and DE(is the cumulative number of ruptured sub-faults by the time rupture reaches the jth sub-fault. The spatial modifying function D(f) is given by;

$$D(r,f) = G \exp\left[\frac{-\pi f r}{V_s Q(f)}\right] \quad (10)$$

where, G is the geometric attenuation factor. The other term denotes anelastic attenuation with hypo-central distance r and the quality factor as Q. The spatial spread of the ground motion depends sensitively on the quality factor of the local region. The constant C of equation (7) is;

$$C = \frac{\langle R_{\theta\phi}\rangle\sqrt{2}}{4\pi\rho V_s^3} \quad (13)$$

where, $<R\Theta\phi>$ is the radiation coefficient averaged over an appropriate range of azimuths and take -off angles and ρ is the material density at the focal depth. The coefficient $\sqrt{2}$ in the above equation arises as the product of the free surface amplification and partitioning of energy in orthogonal directions. The scaling factor for j^{th} sub-fault, H_j based on the squared acceleration spectrum is taken as (Boore 2009).

$$H_j = \sqrt{N}\,\frac{f_0^2}{f_{0j}^2} \quad (12)$$

where, f0 is the corner frequency at the end of the rupture which can be obtained by substituting NR (t) = N in equation (9). The filter function Pj(f) is taken as;

$$P_j(f) = \frac{\sqrt{N}}{H_j}\,\frac{1+\left(f/f_{0j}\right)^2}{1+(f/f_0)^2} \quad (13)$$

The moment of jth sub-fault is computed from the slip distribution as follows

$$M_{0j} = \frac{M_0 D_j}{\sum_{(j=1)}^{N} D_j} \quad (14)$$

Here, D_j is the average final slip acting on the j^{th} sub-fault and M_0 is the total seismic moment on the fault. To further account for earthquake rupture Motazedian and Atkinson (2005) introduced the concept of pulsing area where the cumulative number of active sub-faults, N_{Rj} increases with time at the initiation of rupture and becomes constant at some fixed percentage of the total rupture area. This parameter determines the number of active sub-faults during the rupture of j^{th} sub-fault.

As a result, N_{Rj} sub-faults will be considered for computing the corner frequency f_{0j} given in equation 9. The above is a general finite source model expressed in the frequency domain, valid for any region if only the various controlling parameters can be selected suitably. Since, almost all the required parameters for India have been worked out in the past by geophysicists and seismologists using various types of instrumented data from small and large earthquakes, the above method can be conveniently carried out. The spatial modifier of equation (10) consists of a general geometrical attenuation term *G*. This is taken following Singh *et al.* (1999) as

mani $$G = \begin{cases} \frac{1}{r}, & for\ r \leq 100 \\ \frac{1}{10\sqrt{r}}, & for\ r > 100 \end{cases} \quad (15)$$

The shear wave velocity and density at the focal depth are fixed at 3.6 km/s and 2900 kg/m3 respectively for both the active regions corresponding to compressed hard granite (NDMA 2011). In the past, seismologists have analyzed instrumental data to arrive at estimates of the frequency dependent quality factor in these active regions. Large amount of literature exists on the estimation of these parameters. Singh et al (2004) have studied the 1991 Uttarkashi earthquake and 1999 Chamoli earthquake and derived the quality factor for Himalayan region as 253 $f^{0.8}$. Mohanty *et al.* (2009) studied the strong motion data of 55 earthquakes of magnitude 1.5 to 4.2 acquired from Delhi telemetric network and derived the Quality factor for Indo-Gangetic plain as 142 $f^{0.8}$. The regional velocity model for Himalayan region used is the one reported by Parvez *et al.* (2003). Details of the regional model are presented in Figure 53. Modification between bedrock and A-type site is a linear problem in one-dimension and hence for such sites, amplification function *[F(f)]* in equation (7) can be directly found by the quarter-wavelength method of Boore and Joyner (1997). The estimated amplification function is presented in Figures 54.

The other important regional parameter is the focal depth which can vary from as low as 5 km to as deep as 100 km or more. The variation in focal depth is fairly well known for the different regions in India (Shukla *et al.* 2007; Kayal 2008). The range of focal depth, stress drop and dip in the two regions are reported in Table 6. Apart from the above parameters, the S-wave radiation coefficient *(<RΘϕ>)* varies randomly within particular intervals. Here, following Boore and Boatwright (1984), the S-wave radiation coefficient is taken to be in the interval 0.48–0.64. In addition to the above parameters the pulsing percentage area is also required in the simulation. The pulsing percentage area is varied from 25% - 75%.

1.8.2 Sample Ground Motion

From the above discussion it is seen that once the stress drop, quality factors for the region are known, then the Fourier amplitude spectrum of ground acceleration for a given magnitude (M_w) and hypocentral distance *(r)* can be expressed within the limitations of a finite source seismological model. Since, this is a random process and hence in time domain, this represents an ensemble of accelerograms. These samples can be retrieved from equation (7) in three steps. First, a Gaussian stationary white noise sample of length equal to the strong motion duration (Boore and Atkinson 1987)

$$T = \left(\frac{1}{f_c} + 0.05\, r\right) \quad (16)$$

is simulated for each sub-fault. This sample is multiplied by a suitable non-stationary modulating function suggested by Saragoni and Hart (1974). The simulated sample is Fourier transformed into the frequency domain. This Fourier spectrum is normalized by its root mean-square value and multiplied by the seismological source-path-site function A(f) of equation (7). The resulting function is transformed back into the time domain toget a sample of the ground motion accelerogram for each sub-fault. The simulated acceleration time histories for all the sub-faults are summed up with time delay of Δt to account for the rupture velocity to obtain the final ground acceleration expressed as,

$$a(t) = \sum_{j=1}^{N} a_j\left(t + \Delta t_j\right) \quad (17)$$

Any number of accelerograms can be simulated in this fashion to compute samples of response spectra corresponding to 5% damping.

1.8.3 Site Amplification Function

The surface level ground motion at a given site is the rock motion modified by the soil layers. The local property of the top layers is conveniently expressed in terms of the average shear wave velocity in the top 30 meters of the soil. It is observed from Table 5 that the sites in HP can be classified into C-type and D-type sites. The general approach of finite source seismological model described above can be extended to C- and D-type sites with the help of depth sections sampled from the region with known V_s values. In addition to the uncertainties in the magnitudes and epicentral distances, one has to consider the variations in the soil profiles also for simulating spectral accelerations at the ground surface. Thus, for a specific site, modification of the bedrock results is possible with the help of variation of V_s with depth. The shear wave velocity profiles obtained from MASW test at 73 locations are used to estimate site amplification functions. Modification of acceleration time history between bedrock and soil site is a nonlinear problem in one dimension and hence for such sites, amplification can be directly found by the nonlinear site response analysis (Idriss and Sun, 1992). The main assumption in one-dimensional site response analysis is that the response in a soil deposit is caused by upward propagation of shear waves from the underlying rock formation to the overlying soil mass. The nonlinear behaviour of the soil, characterized in terms of reduction of shear modulus and increase of damping ratio with shear strain, can be accounted by using equivalent linear soil properties. For this purpose, shear modulus reduction versus shear strain curves and damping ratio versus shear strain curves, need to be developed. However, in the present analysis, the standard curves proposed by Vucetic and Dobry (1991) for different type of soils i.e., clay, sand and rock, have been used. Based on the borelog information and visual observation, the soil for different layers are classified as clay, sand etc. Nonlinear site response analysis can be conveniently carried out using the computer program SHAKE91 of Idriss and Sun (1992). The frequency response function (FRF) defined as the surface response for a rock level sinusoidal motion of unit amplitude is estimated from SHAKE91 for all the 73 shear wave velocity profiles. These functions for both C-type and D-type sites are shown in Figure 55 and 56.

1.8.4 Synthetic Ground Motion Database

Here spectral acceleration values have been simulated for moment magnitude (M_w) ranging from 4 to 8.5 in increments of 0.5 units, at 20 values of hypo-central distances ranging from 1 to 500 km. To capture finiteness of the source the ground motions are also simulated for eight azimuths ranging from 0^0 to 315^0 in increments of 45^0. Thus a total number of 160 distance samples are considered for each magnitude. In all, there are 1600 pairs of magnitudes and distances. Since the stress drop, focal depth, dip, radiation coefficient and pulsing percentage area are random variables, we have included the uncertainty arising out of these parameters also. It can be observed from Table 5 that there are 50 C-type sites and 21 D-type sites in HP. For uniformity, a random sample of 29 D-type shear wave velocity profiles are generated by varying the obtained D-type shear wave velocity profiles in HP. The uncertainty associated with the local site amplification has to be included to develop ground motion relations. Fifty samples of stress drop, focal depth, dip, radiation coefficient, pulsing percentage area and shear wave velocity profiles are generated and these are combined using the Latin Hypercube sampling technique (Iman and Conover 1980) to select for each magnitude value fifty sets of random seismic

parameters. The acceleration time histories are first simulated for A-type site using the amplification function shown in Figure 54. The simulated time history combined with the randomly generated shear wave velocity profile is used as an input to SHAKE91 to obtain the surface level response spectrum. Thus, a database of 80,000 PGA and Sa samples corresponding to 1600 simulated earthquake events are generated. This synthetic database is developed separately for both Himalayan and Indo- Gangetic regions for both C-type and D-type site condition.

1.8.5 Ground motion relations

Several functional forms of ground motion attenuation have been proposed in the literature for reflecting salient aspects of the spread of ground motion (Sadigh *et al*. 1997, Toro *et al*. 1997, Campbell 2003, Atkinson and Boore 2006). Since all the proposals are empirical the particular form selected are justified heuristically and sometimes by limited comparison with instrumental records. After reviewing the various available forms of equations, it has been decided to develop the attenuation relation for all the four active regions in the form

$$\ln\left(\frac{S_a}{g}\right) = c_1 + c_2 M + c_3 M^2 + c_4 r + c_5 \ln\left(r + c_6 e^{c_7 M}\right) + c_8 \log(r) f_0 + \ln(\varepsilon) \qquad (18)$$

$$f_0 = \max(\ln(r/100), 0)$$

Here S_a is the spectral acceleration, M is the moment magnitude, r is the hypocentral distance in kilometers. This form of the attenuation accounts for geometrical spreading, anelastic attenuation and magnitude saturation similar to the finite source seismological model discussed previously. The coefficients of the above equation are obtained from the simulated database of 80,000 samples by regression analysis. The coefficients c1-c8 and the standard error are shown in Tables 7-10 as functions of natural period for C-type and D-type site condition in Himalayan and Indo-Gangetic regions. These results can be used to construct the mean and (mean + sigma) response spectrum in the two active regions of India. In Figs. 57 & 58, the attenuation of PGA in the Type-C & -D sites respectively in the Himalayan regions is shown for different magnitude values. In Figs. 59 & 60, the attenuation of PGA in the Type-C & -D sites respectively in the Indo-Gangetic region is shown for different magnitude values. Figure 61 and 62 shows the response spectra for M_w 7 event of Himalayan and Indo-Gangetic region at epicentral distances of 10 km and 100 km respectively. The response spectra for both C-type and D-type condition are shown in the same figure.

1.9 Probabilistic Seismic Hazard Analysis (PSHA)

After deriving the zonal level earthquake recurrence relation and ground motion relations the next step in PSHA is to estimate the probability of exceedance of ground motion by integrating the uncertainties in source, path and site.

1.9.1 Fault Deaggregation

In section 6, the recurrence relations have been derived for six seimogenic zones and are not specific to any particular fault. Fault-level recurrence is necessary to discriminate nearby sources from far-off sources and to differentiate activity rate among faults. Such fault-level recurrence relation is rarely known due to paucity of large-scale data accruing in historical times. An alternative is to empirically fix the b-value by measuring the slip rate of a fault. For the faults under consideration, no slip values are available. Hence, one

has to proceed on a heuristic basis invoking the principle of conservation of seismic activity. A simple principle based on conservation of seismic activity which states that the regional seismicity value quantified as $N(m_0)$ (number of earthquakes per year with $m>m_0$) should be equal to the sum of individual fault value $N_k(m_0)$ ($k=1,2,..N_f$;) where N_f is the number of faults in seismogenic zone), is invoked for estimating the recurrence relation. To incorporate past activity in a weighted fashion, a weighting factor (χ_k) is obtained by distributing the total number of past data to individual faults. This assumes that past seismicity patterns will continue in future also. Another weighting factor (α_k) proportional to length of the fault is introduced to distribute the regional seismicity. To compensate between the above two different assumptions, a composite weightage represented as (NDMA 2011) is used.

$$N_k(m_0)=0.5(\alpha_k+\chi_k)\, N(m_0) \quad (k=1,2,...N_f) \tag{19}$$

Here α_k is ratio of the length of fault k to the total length of all the faults and χ_k is ratio of the number of past earthquakes greater than magnitude 4 and above attributed to fault k to the total number of earthquakes in the region. N_f is the number of faults in the region. Assuming the *b*-value of each fault to be same as that of regional b-value, the recurrence relation for any fault *k* will be

$$N_k(m) = N_k(m_0)\left[\frac{1-e^{-\beta(m-m_0)}}{1-e^{-\beta(m_u-m_0)}}\right] \tag{20}$$

Here m_u is the maximum magnitude of fault *k* and $\beta=2.303b$. This assumption amounts to taking that each fault is as active as the region itself. Figure 63 shows the recurrence relation for each of the 97 faults obtained from equation 20 in the seismogenic zone 1.

1.9.2 Seismic Hazard Analysis

Probabilistic seismic hazard analysis estimates the probability of exceedance of various ground motion levels at a site given all possible earthquakes. The basic formulation for PSHA has been derived by Cornell (1968) assuming point source model for earthquakes. Later Kiureghian and Ang (1977) improved PSHA to include finite source size and other uncertainties. In the recent years, PSHA has become a standard tool for estimating ground motion. The procedure required for PSHA has been discussed in detail in the literature (Kramer 1996; EM 1110-2-6050). A similar methodology has been followed in the present study also. Based on the total probability theorem, the probability of exceedance of a particular value y* can be computed using the equation

$$P[Y > y^*] = \int_{m=m_0}^{m_u}\int_{r=r_{min}}^{r_{max}} P[Y > y^*|r,m]p_{R|M}(r|m)p_M(m)\,dr\,dm \tag{21}$$

where, $p_M(m)$ is the probability density function of the magnitude. m_0 and m_u are the threshold magnitude and maximum magnitude of the fault. $P[Y > y^*|r, m]$ denotes the conditional probability that the chosen ground motion level is exceeded for a given magnitude and distance. r_{min} and r_{max} are the minimum and maximum site distances from the fault. $p_{R|M}(r|m)$ is the conditional probability density function of hypocentral distance. The expression for the cumulative probability distribution to a linear rupture segment uniformly distributed along a linear fault situated entirely to one side of a site can be expressed as (Kiureghian and Ang 1977)

$$P(R < r|m_i) = 0 \qquad for\ R < \sqrt{(D^2 + L_0^2)}$$
$$P(R < r|m_i) = \frac{(r^2 - D^2)^{1/2} - L_0}{L - X(m_i)} \qquad for\ r_0 \le R < \sqrt{D^2 + [L + L_0 - X(m_i)]^2}$$
$$P(R < r|m_i) = 1 \qquad for\ R > \sqrt{D^2 + [L + L_0 - X(m_i)]^2} \qquad (22)$$

where L,X, h, r0 and r are the length of the fault, fault rupture length, focal depth minimum distance of the site to the fault and minimum distance of the site to the fault rupture respectively. Here, D is the perpendicular distance of the site to the fault and d=√D2-h2.X(m) is the rupture length and is given by the equation (Wells and Coppersmith 1994).

$$X(m_i) = \min[10^{-2.44+0.59m_i}, L] \qquad (23)$$

In the above equation min is used to confine the rupture to the fault length. If the fault is extending on both sides of the source, the conditional distance probabilities for the two sides are found separately, multiplied by the fraction of the length of corresponding sites and summed up to the desired probability. Equation 21 can be computed numerically by assuming that a fault is capable of generating earthquakes of discrete magnitudes mi, separated by Δm and only at some discrete source to site distances rj, separated by Δr which can be written as

$$P[Y > y^*] = \sum_{i=1}^{N_m} \sum_{j=1}^{N_r} P[Y > y^*|r_j, m_i] P[r_j|M = m_i] P[M = m_i] \qquad (24)$$

where,

$$r_j = r_{min} + \left(j - \frac{1}{2}\right)\Delta r; m_i = m_0 + \left(i - \frac{1}{2}\right)\Delta m; N_r = \frac{r_{max} - r_{min}}{\Delta r}; N_m = \frac{m_u - m_0}{\Delta m} \qquad (25)$$

Since at a site there can be several faults, the mean annual rate of exceedance of y* at the site is found by

$$\mu_{y^*} = \sum_{k=1}^{N_f} \sum_{i=1}^{N_m(k)} \lambda_k(m_i) \sum_{j=1}^{N_r(k,i)} P[Y > y^*|r_{k,ij}, m_{k,i}] P[r_j|M = m_{k,i}] \qquad (26)$$

where, N_f is the number of faults. In the above equation, the frequency of occurrence of events of magnitude m_i of the k^{th} fault, $\lambda k(m_i)$ is related to the probability density function of the magnitude and can be expressed as

$$\lambda_k(m_i) = N_k(m_0) P[M = m_{k,i}] \qquad (27)$$

In the above equation and in equation 24

$$\sum_{i=1}^{N_m(k)} P[m_{k,i}] = 1 \qquad (28)$$

$$\sum_{i=1}^{N_r(k,i)} P[r_{k,ij|M=m_{k,i}}] = 1 \qquad (29)$$

The frequency of occurrence of events can be computed from the following expression as

$$\lambda_k(m_i) = N_k\left(m_i - \frac{\Delta m}{2}\right) - N_k\left(m_i + \frac{\Delta m}{2}\right) \qquad (30)$$

Where,

$$N(m) = N(m_0)\frac{e^{-\beta(m-m_0)} - e^{-\beta(m_u-m_0)}}{1 - e^{-\beta(m_u-m_0)}} \quad (31)$$

Since, peak ground acceleration (PGA) is known to be nearly distributed as a log-normal random variable, the probability of ground motion exceedance for a given magnitude and epicentral distance is computed from the expression

$$P[Y > y^*|r_{k,ij}, m_{k,i}] = 1 - \Phi'\left\{\frac{\ln(y^*) - E[\ln(y_s)]}{\sigma[\ln(\epsilon_s)]}\right\} \quad (32)$$

where, *E[ln(ys)]* and *σ(ln εs)* are the mean and standard deviation of the logarithm of ground motion at site s given by the attenuation relation (eq. 18) and Φ' represents the cumulative truncated normal distribution.

$$\Phi'(U) = \frac{\Phi(U) - \Phi(-3)}{1 - 2\Phi(-3)} \quad (33)$$

where, Φ(*U*) is the standard cumulative normal distribution, *U* is the standard normal variate and Φ (-3) is 0.00135. The above three probabilities are calculated for all possible source to site distances and magnitudes on each fault. The mean annual rate of exceedance of *y** is obtained by summing over the individual probabilities due to all faults. This is repeated for various ground motion values *y** to obtain the seismic hazard curves. Assuming that the number of earthquakes occurring on a fault follows a stationary Poisson process, the probability of exceedance of *y**, in a particular time period T years is given by

$$P(Y > y^* \text{ in T years}) = 1 - e^{-\mu_{y^*}\cdot T} \quad (34)$$

It can be observed from the above equation that as design life increases, the probability ofexceeding particular values also increases. As a result, the value of the design ground motion parameter also increases with increase in T. The reciprocal of the annual probability of exceedance gives the return period for the corresponding ground motion value.

In Figures 64-82, the seismic hazard curves for PGA at 12 district headquarters in HP is shown. For cities such as Shimla, the hazard curves for both C and D-type sites are reported. In Table 11, the obtained PGA values corresponding to 25, 50, 100, 200, 475 and 2475-year return periods are reported at 73 test sites.

Traditionally, PGA has been used to characterize ground motion in PSHA. Presently, the preferred parameter is the response spectral acceleration (Sa). The response spectrum, which has the same level of hazard or annual probability of exceedance at all frequencies, is known as uniform hazard response spectrum (UHRS). To derive UHRS for 12 district headquarters in HP, PSHA is performed on spectral acceleration, at 27 natural period values, using the coefficients reported in Tables 6-9. From these seismic hazard curves, spectral acceleration values are taken corresponding to 475-year and 2475-year return periods. UHRS computed for above two hazard levels are plotted in Figures 83-101 for important cities in HP. The derived UHRS for C- and D-type site shows a dominant peak at 15 Hz.

Probabilistic seismic hazard analysis for PGA, and spectral accelerations corresponding to periods 0.2 and 1 seconds has been carried out for all the grid points at a resolution of 0.01^0 x 0.01^0 spread over the HP. The final results valid for C-type and D-type sites are

presented as contour maps for return periods 25, 50,100,200, 475 and 2475 years. These are shown in Figures 102-107 for Type-C site and in Figures 120-125 for Type-D site. For developing design response spectrum as per the International Building Code (IBC2003), one needs spectral acceleration values at 0.2-second and 1-second periods. These results are shown in Figures 108-119 and in Figures 126-137 for Type-C & -D sites respectively.

Chapter 2: Conclusions

Hazard maps for PGA and spectral acceleration have been derived for HP by performing detailed PSHA. A circular region of radius 500 km around the target sites is taken and more than 195 faults have been considered in estimating the future seismic hazard. The seismic hazard for HP is mainly controlled by the MCT and MBT faults in the Himalayan region. The recurrence relation for the seismic zones is found from the maximum likelihood method of Kijko and Sellevoll (1989) including incompleteness and uncertainty of the database. New ground motion relations including local soil conditions are derived for Himalayan and Indo-Gangetic regions. Detailed seismic hazard curves have been computed considering all the uncertainties. From these seismic hazard curves response spectra corresponding to 25-year, 50-year, 100-year, 200-year, 475-year, and 2475-year return periods have been found. Uniform hazard response spectra for twelve important cities have been obtained from PSHA. The obtained results can be further used for seismic design for new structures in HP. The obtained hazard curves combined with UHRS can be used to construct risk maps for HP.

Chapter 3: References

Algermissen, S.T. and Perkins, D.M. (1976), *A probabilistic estimate of maximum acceleration in rock in the contiguous United States*, U.S. Geol. Surv, Open-file Report, 76–416, pp. 45.

Ambraseys, N. and Bilham, R. (2009), The tectonic setting of Bamiyan and seismicity in and near Afghanistan for the past twelve centuries. UNESCO Special Publication: The Destruction of the Giant Buddha Statues in Bamiyan, Central Afghanistan, UNESCO's emergency activities for the recovering and rehabilitation of cliff and niches. Ed. Claudio Margottini, ISBN 978-448-0375-5. 158 p.

Ambraseys, N. and Jackson, D. (2003), A note on early earthquakes in northern India and southern Tibet, Curr. Sci., 84, pp. 570-582.

Anderson, J.G. and Trifunac, M.D. (1978), Uniform risk functional for characterization of strong earthquake ground motion, Bulletin of the Seismological Society of America, 68(1), pp. 205–218.

Atkinson G. M., Boore D. M. (1995). Ground-motion relations for eastern North America, Bulletin of the Seismological Society of America, 85(1), pp. 17-30.

AERB (1990), Seismic Studies and Design Basis Ground Motion For Nuclear Power Plant Sites, AERB Guide No. AERB/SG/S-11, Atomic Energy Regulatory Board, Vikram Sarabhai Bhavan, Bombay, India.

Bapat, A. Kulkarni, R.C. and Guha, S.K. (1983). Catalogue of earthquakes in India and Neighborhood from historical period up to 1799, Indian Society of Earthquakes Technology, pp. 211.

Balakrishnan, T. S., Unnikrishnan, P., and Murthy, A.V.S. (2009). The tectonic map of India and contiguous areas, Journal of Geological Society of India. 74, pp. 158-170.

Baumbach, M., Grosser, H., Schmidt, H.G., Paulat, A., Rietbrock, A., Ramakrishna Rao, C.V., Solomon Raju, P., Sarkar, D. and Mohan, I. (1994), Study of foreshocks and aftershocks of the intraplate Latur earthquake of September 30, 1993, India; In: Latur Earthquake (ed) H K Gupta, Geol. Soc. India Mem., 35, pp. 33-63.

Bhatia, S.C., Kumar, M.R. and Gupta, H.K. (1999), A probabilistic seismic hazard map of India and adjoining regions, Annali di Geofisica, 42, pp. 1153-1166.

Bilham, R. (2004), Earthquakes in India and the Himalaya: tectonics, geodesy and history, Annals of Geophysics, 47(2), pp. 839-858.

Bilham, R. and Szeliga, W. (2008), Interaction between the Himalaya and the flexed Indian plate-spatial fluctuations in seismic hazard in India in the past millennium?, 2008 Seismic enginering conference commemorating the 1908 Messina and Reggio Calabria earthquake. Santini A, Moraci N (eds) American Institute of Physics Conference Proceeding 1020(1), pp. 224–231, (978-0-7354-0542-4/08).

Bodin, P. *et al.* (2004), Ground motion scaling in the Kachchh basin, India, deduced from aftershocks of the 2001 M_w 7.6 Bhuj earthquake, Bulletin of the Seismological Society of America, 94(5), pp. 1658-1669.

Boore, D. M. (1983). Stochastic simulation of high-frequency ground motions based on seismological models of the radiated spectra, Bulletin of the Seismological Society of America, 73, 1865-1894.

Boore, D.M. (2003), Simulation of ground motion using the stochastic model, Pure and Applied Geophysics, 160, pp. 635 – 676.

Boore, D.M. (2009). Comparing stochastic point-source and finite-source ground motion simulations: SMSIM and EXSIM, Bulletin of the Seismological Society of America, 99(6), pp. 3202-3216.

Boore, D. M. and Atkinson, G.M. (1987), Stochastic prediction of ground motion and spectral response parameters at hard-rock sites in Eastern North America, Bulletin of the Seismological Society of America, 77, pp. 440–467.

Boore, D. M. and Boatwright, J. (1984), Average body wave radiation coefficients; Bulletin of the Seismological Society of America, 74, pp. 1615–1621.

Boore, D.M., and Joyner, W.B. (1997), Site amplifications for generic rock sites, Bulletin of the Seismological Society of America, 87(2), pp. 327-341.

Brune, J.N. (1970), Tectonic stress and spectra of seismic shear waves from earthquakes, Journal of Geophysical Research, 75, pp. 4997 – 5009.

Campbell, K. W. (2003), Prediction of Strong Ground Motion Using the Hybrid Empirical Method and Its Use in the Development of Ground-Motion (Attenuation) Relations in Eastern North America, Bulletin of the Seismological Society of America, 93(3), pp. 1503-1606.

Chandra, U. (1978), Seismicity, earthquake mechanisms and tectonics along the Himalayan mountain range and vicinity, Phys. Earth Planet. Inter., 16, pp. 109-131.

Chandra, U. (1992), Seismotectonics of Himalaya, Current Science, 62 (1–2), pp. 40–71. Chandrasekaran, A.R. and Das, J.D. (1992), Strong motion arrays in India and analysis of data from Shillong array, Current Sci., 62, pp. 233-250.

Chen, W. P. and Molnar, P. (1990), Source parameters of earthquakes and intraplate deformation beneath the Shillong Plateau and northern Indoburman Ranges, J. Geophys. Res., 95, pp. 12527-12552.

Cornell (1968), Engineering seismic risk analysis, Bulletin of the Seismological Society of America, 58(5), pp. 1503-1606.

Cornell, C.A. (1970), Probabilistic analysis of damage to structures under seismic loads. In Dynamic Waves in Civil Engineering, Chapter 27, Howells DA, Haigh IP, Taylor C (eds). Wiley-interscience: New York, 1970; Proceedings of Conference on Earthquake and Civil Engineering Dynamics, University College at Swansea, 7–9 July 1970.

Cornell, C.A. and Merz, H. A. (1974). Seismic risk analysis of Boston, Journal of Structural Division, ASCE, 101, pp. 2027-2043.

Der Kiureghian, A. and Ang, A. H.-S. (1977), A fault rupture model for seismic risk analysis, Bulletin of the Seismological Society of America, 67, pp. 1173–1194.

DOE STANDARD (1996), Natural phenomena hazards performance categorization guidelines for structures systems and components, DOE-STD-1021-93, US Dept. of energy, Washington, D.C.

EM 1110-2-6050, Response Spectra and Seismic Analysis for Concrete Hydraulic Structures, U.S. Army Corps of Engineers Washington, DC, pp. 20314-1000.

Fitch, T.J. (1970), Earthquake mechanisms in the Himalaya, Burmese, and Andaman regions and continental tectonics in Central Asia, J. Geophys. Res., 75, pp. 2699–2709. Frankel, A. (1995), Mapping seismic hazard in the Central and Eastern United States, Seismological Research Letters, 66(4), pp. 4–8.

Frankel, A. (1995). Simulating strong motion of large earthquakes using recordings of small earthquakes: the Loma Prieta Mainshock as test case. Bulletin of the Seismological Society of America, 85, pp. 1144-1160.

Gansser, A. (1974), The Ophiolitic Melange, a world-wide Problem on Tethyan examples, Eclogae geol. Helv., 67, pp. 479-507.

Gardner, J.K. and Knopoff, L. (1974), Is the sequence of earthquakes in Southern California, with aftershocks removed, Poissonian?. Bulletin of the Seismological Society of America, 64, pp. 1363–1367.

Gaull, B.A., Michael-Leiba, M.O. and Rynn, J.M.W. (1990), Probabilistic earthquake risk maps of Australia, Australian Journal of Earth Sciences, 37, pp. 169-187.

Giardini, G., Wiemer, S., Fäh, D. and Deichmann, N. (2004), Seismic Hazard Assessment of Switzerland, Publication Series of the Swiss Seismological Service, ETH Zürich, 91 p.

GSI (2000), Seismo-tectonic Atlas of India and its Environs, Geological survey of India, 2000.

IBC (2003), International Building code, International Code Council, ICC.

Idriss, I.M. (1985), Evaluating seismic risk in engineering practice. Proc. of the 11th Intl. Conf. on Soil Mechanics and Foundation Engineering, San Francisco, 1, pp. 255–320. Iman, R.L. and Conover, W.J. (1980), Small sample sensitivity analysis techniques for computer models, with an application to risk assessment, Communications in Statistics, A9(17), pp. 1749-1842. Rejoinder to Comments, pp. 1863-1874.

IS 1893-2002 (2002), Criteria for earthquake resistant design of structures: Part 1 - General provisions and buildings, Bureau of Indian Standards, BIS, New Delhi.

Iyengar, R.N, Sharma, D, and Siddiqui, J.M. (1999), Earthquake history of India in medieval times, Indian Journal of history Science, 34 (3).

Iyengar, R.N. and Raghukanth, S.T.G. (2004), Attenuation of strong ground motion in peninsular India, Seismological Research Letters, 75(4), pp. 530-540.

Iyengar, R.N., Ghosh, S. (2004), Micro-zonation of earthquake hazard in Greater Delhi area, Current Science, 87(9).

NDMA (2011), Development of probabilistic seismic hazard map of India. A Technical report of the Working Committee of Experts (WCE) constituted by the National Disaster Management Authority (NDMA), Govt. of India, New Delhi.

Joyner, W.B. and Boore, D.M. (1981), Peak horizontal acceleration and velocity from strong-motion records including records from the 1979 Imperial Valley, California, Earthquake, Bulletin of the Seismological Society of America, 71, pp. 2011–2038.

Kaila, K.L., Gaur, V.K. and Narain Hari (1972), Quantitative seismicity maps of India. Bulletin of the Seismological Society of America, 62, pp. 1119–1131.

Kanamori, H. and Anderson, D. L. (1975), Theoretical basis of some empirical relations in seismology, Bulletin of the Seismological Society of America, 65, pp. 1073-1095.

Kayal J.R. (2008), Microearthquake Seismology and Seismo-tectonics of South Asia. Capital Publishing Company, New Delhi.

Khattri, K.N. (1994), Earthquake hazard in Indian region, Sadhana, 19(4), pp. 609-614. Khattri, K.N., Rogers, A.M., Perkins, D.M. and Algermissen, S.T. (1984), A seismic hazard map of India and adjacent areas, Tectonophysics, 108, pp. 93–134.

Kijko A. and M.A. Sellevoll (1989), Estimation of earthquake hazard parameters from incomplete data files. Part I. Utilization of extreme and complete catalogs with different threshold magnitudes, Bulletin of the Seismological Society of America, 79, pp. 645-654.

Kijko, A. and Graham, G. (1998), Parametric-historic procedure for probabilistic seismic hazard analysis: Part I - estimation of maximum regional magnitude mmax, Pure Appl. Geophys., 152, pp. 413-442.

Kijko, A. and Graham, G. (1999), "Parametric-historic" procedure for probabilistic seismic hazard analysis, Part II: assessment of seismic hazard at specified site, Pure and Appl. Geophys., 154, pp. 1–22.

Kijko, A. (2002), Statistical estimation of maximum regional magnitude mmax. In: Proceedings of the 12th European Conference on Earthquake Engineering, London, Sept. 9-13, Elsevier Science, paper Reference FW:022.

Kiureghian, Der A., and Ang, A. H.S. A fault rupture model for seismic risk analysis,

Bulletin of the Seismological Society of America, 67(4), pp. 1173-1194.

Knopoff, L. and Kagan, Y. (1977), Analysis of the theory of extremes as applied to earthquake problems, J. Geophys. Res., 82, pp. 5647-5657.

Kramer, SL (1996), Geotechnical Earthquake Engineering, Prentice Hall, Inc., Upper

Saddle River, New Jersey, USA.

Kumar, S., Wesnouskey, S.G., Rockwell, T.K., Ragona, D., Thakur V.C. and Seitz, G.G. (2001), Earthquake reoccurrence and rupture dynamics of Himalayan Frontal Thrust, India, Science, 294, pp. 2328–2331.

Lave, J., Yule, D., Sapkota, S., Basant, K., Madden, C., Attal, M., Pandey, R. (2005), Evidence for a great medieval earthquake (1100 A.D.) in the Central Himalayas, Nepal. Science, 307, pp. 1302–1305.

Mai, P.M., and G.C. Beroza (2000), Source-scaling properties from finite-fault rupture models, Bulletin of the Seismological Society of America, 90, pp. 604-615.

Malik, J.N., Nakata, T., Philip, G. and Virdi, N.S. (2003), Preliminary observations from trench near Chandigarh, NW Himalaya and their bearing on active faulting. Current Science, 85 (12), pp. 1793-1799.

McCalpin, J. (2009), Paleoseismology, Volume 95 of International geophysics series, Academic Press, 2nd Edition, 613 p.

Milne, J. (1911), A catalogue of destructive earthquakes: A.D. 7 to A.D. 1899, British Association for the Advancement of Science London, 92 p.

Mohanty, W.K., Prakash, R., Suresh, G., Shukla, A.K., Walling, M.Y. and Srivastava, J.P. (2009), Estimation of coda wave attenuation for the national capital region, Delhi, India using local earthquakes, Pure and Applied Geophysics, 166(3), pp. 429-449.

Nandy D. R. (1995), Neotectonism and Seismic Hazards in India, Indian J. of Geology, 67 (1), pp. 34-48.

Newmark, N. M., John A. Blume, and Kanwar K. Kapur (1973), Seismic Design Spectra for Nuclear Power Plants, J. Power Division, ASCE, 99(2), pp. 287-303.

Oldham, T. (1883), A catalogue of Indian earthquakes from the earliest times to the end of 1869 A.D., Mem. Geol. Surv. India. XIX, Part. 3.

Parvez, I.A., Vaccari, F. and Panza, G.F. (2003), A deterministic seismic hazard map of India and adjacent areas. Geophysical Journal International, 155, pp. 489-508

PMD (2007), Seismic Reports, Pakistan Meteorological Department, url: www.pakmet.com.pk

Quittmeyer, R.C. and Jacob, K.H. (1979), Historical and modern seismicity of Pakistan, Afghanistan, north-western India and south-eastern Iran, Bulletin of the Seismological Society of America, 69, pp. 773-823.

Raghukanth S.T.G. and Iyengar R.N. (2006), Seismic hazard estimation of Mumbai city, Current Science, 92(11), pp. 1486-1494.

Raghukanth, S.T.G and Iyengar, R.N. (2007), Estimation of seismic spectral acceleration in Peninsular India, Journal of Earth System Science, 116(3), pp. 199 – 214.

Reasenberg, P. (1985), Second-order moment of central California seismicity, 1969 1982, J. Geophys. Res. 90, pp. 5479–5495.

Sadigh, K., Chang, C. Y., Egan, J. A., Makdisi, F., and Youngs, R. R., (1997).

Attenuation relationships for shallow crustal earthquakes based on California strong motion data, Seismol. Res. Lett. 68, pp. 180–189.

Saragoni, G.R. and Hart, G. C. (1974), Simulation of artificial earthquakes, Earthq. Eng. Struct. Dyn., 2, pp. 249–267.

Scordilis, E. M. (2006), Empirical global relations converting Ms and Mb to moment magnitude. Journal of Seismology, 10, pp. 225-236.

Seeber, L., Armbruster, J.G. and Jacob, K.H. (1999), Probabilistic assessment of earthquake hazard for the state of Maharashtra. Report to Government of Maharashtra Earthquake Rehabilitation Cell Mumbai.

Shanker, D. and Sharma, M.L. (1998), Estimation of seismic hazard parameters for the Himalayas and its vicinity from complete data files, Journal of Pure and Applied Geophysics, 152(2), pp. 267-279.

Sharma, M.L. (1998), Attenuation relationship for estimation of peak ground horizontal acceleration using data from strong-motion arrays in India, Bulletin of the Seismological Society of America, 88, pp. 1063-1069.

Shukla, A. K., Prakash, R., Singh, R. K., Mishra, P.S. and Bhatnagar, A. K. (2007), Seismotectonic implications of Delhi region through fault plane solutions of some recent earthquakes, Current Science, 93(12), pp. 1848-1853.

Singh, S.K., Garc, D., Pacheco, J.F., Valenzuela, R., Bansal, B.K. and Dattatrayam, R.S. (2004), Q of the Indian Shield, Bulletin of the Seismological Society of America, 94(4), pp. 1564-1570.

Stepp J. C. (1972), Analysis of Completeness of the Earthquake Sample in the Puget sound area and its effect on statistical estimates of earthquake hazard, International Conference on Microzonation, vol. II, pp. 897-909.

Tandon, A. N. & Chaudhury, H. M. (1968). Koyna earthquake of December, 1967, India Meteorol. Dept., Scientific Report No. 59.

Toro G., N. Abrahamson, and J. Schneider (1997), Model of strong ground motion in pp. 41-57.

Turner, H.H. (1911), Seismological investigations XII, seismic activity, 1899–1903 inclusive, British Association for the Advancement of Science, London, pp. 57–65.

Umesh Chandra (1977). Earthquakes of Peninsular India-A Seismotectonic Study. Bulletin of the Seismological Society of America, 67(5), pp. 1387-1413.

USNRC (1973), Design response spectra for seismic design of nuclear power plants, Regulatory guide 1.60.

USNRC (1997), Regulatory guide 1.165: Identification and characterization of seismic sources and determination of safe shutdown earthquake ground motion, Report No. DG-1032(RG 1.165), USA.

Valdiya, K.S. (1976), Himalayan transverse faults and folds and their parallelism with subsurface structures of the Northern Indian Plains. Tectonophysics, 32, pp. 353-386. Valdiya, K.S. (2001), Himalaya: emergence and evolution, Universities Press, Hyderabad.

Wadia, D. N. (1957), Geology of India, Macmillan & Co. Ltd., New York.

Wells, J. E., et al (1993), Analysis of the LaSalle Unit 2 Nuclear Power Plant: Risk Methods Integration and Evaluation Program (RMIEP), Vol. 8, NUREG/CR-4832, Lawrence Livermore National Laboratory, Livermore, CA.

Wells, D.L. and Coppersmith, K.J. (1994), Empirical relationships among magnitude, rupture length, rupture width, rupture area and surface displacements, Bulletin of the Seismological Society of America, 84(4), pp. 974-1002.

West, M., & Menke, W. (2000). Fluid-induced changes in shear velocity from surface waves. 13th EEGS Symposium on the Application of Geophysics to Engineering and Environmental Problems (SAGEEP), pp. 21–28.

TARU Leading Edge Pvt. Ltd.
D 406, 4th Floor, Ganesh Meridian,
Opp. Gujarat High Court, S. G. Highway,
Ahmedabad (Gujarat) – 380060 India.

Phone: +91-79-40052401, 40052402
Fax: +91-79-40052400

www.taru.co.in